

## Thoughts and Progress

### Protracted Bleeding After Hirudin Anticoagulation for Cardiac Surgery in a Patient With HIT II and Chronic Renal Failure

\*Ortrud Vargas Hein, \*Christian von Heymann,  
†Stanislao Morgera, ‡Wolfgang Konertz,  
§Sabine Ziemer, and \*Claudia Spies

Departments of \*Anesthesiology and Intensive Care Medicine, †Nephrology and ‡Cardiovascular Surgery and the §Institute of Laboratory Medicine and Pathological Biochemistry, Charité University Hospital Berlin, Campus Mitte, Berlin, Germany

**Abstract:** Heparin-induced thrombocytopenia type II (HIT II) requires alternative anticoagulation. Hirudin has been effectively used in patients with HIT II scheduled for cardiac surgery. However, bleeding complications were observed in patients with renal impairment. In vitro hemodialysis (HD) has been questioned over its efficacy in eliminating hirudin. Another approach to stop bleeding is the application of recombinant factor VIIa (rFVIIa). We report on a patient with HIT II and chronic renal failure who suffered from severe hirudin-induced bleeding after cardiac surgery who was safely treated with a combined approach of surgical hemostasis, substitution of blood products, HD, and rFVIIa to stop finally bleeding. **Key Words:** HIT II—Chronic renal failure—Cardiac surgery—Hirudin—Postoperative bleeding—Hemodialysis—rFVIIa.

Heparin-induced thrombocytopenia type II (HIT II) is a potentially life-threatening complication of heparin therapy because of possible thromboembolism that requires alternative anticoagulation (1). Hirudin, a recombinant direct thrombin inhibitor, has been effectively used in patients with HIT II scheduled for cardiac surgery under inclusion of cardiopulmonary bypass (CPB) (2). However, bleeding complications were observed in patients with renal impairment (2,3). As it is mainly renally excreted, in patients with renal failure an extensive prolongation

of the half-life of hirudin has been described (4). In vitro, high-flux membranes have been used in hemodialysis (HD) for elimination of hirudin, but its efficacy has been questioned as this procedure was insufficient for low plasma concentrations (5,6). In postoperative patients hirudin anticoagulation for continuous renal replacement therapy (CRRT) induced bleeding complications whereas in nonsurgical patients it did not (7,8). Patients with renal failure and HIT II are at high risk of bleeding after surgery. In a recent report on a bivalirudin-induced hemorrhage after heart transplantation, a combined approach using modified ultrafiltration, substitution of fresh frozen plasma, and administration of recombinant factor VIIa (rFVIIa) stopped blood losses successfully (9). Recombinant factor VIIa at various dosages has been reported to be effective in refractory bleeding after cardiac surgery (10,11).

We report on a patient with HIT II and chronic renal failure who suffered a severe hirudin-induced protracted bleed after complex cardiac surgery that was finally and safely treated with a combined approach of surgical hemostasis, substitution of platelets, fresh frozen plasma, high-flux-membrane HD, and rFVIIa.

#### CASE REPORT

A 58-year-old man was admitted to our hospital with mitral valve insufficiency II–III° and aortic valve stenosis III° and was scheduled for mitral valve reconstruction and aortic valve replacement.

The patient's medical history included HIT II. HIT II was diagnosed 5 years before this admission after the patient had suffered two cerebral strokes with a remaining weakness of the left leg without further neurological deficit. He had known chronic renal failure due to analgesic nephropathy and was hemodialyzed 3 times a week with a hirudin bolus of 1–3 mg for dialysis according to a targeted activated partial thromboplastin time (aPTT) > 50 s. The last hemodialysis was performed one day before surgery. The indication for the above mentioned operation was left heart insufficiency (NYHA III), pulmonary hypertension, and angina pectoris because of mitral valve insufficiency II–III° and aortic valve stenosis III°. It was re-do surgery after coronary artery bypass graft surgery (CABG) with postoperative osteomy-

Received October 2004; revised December 2004.

Address correspondence and reprint requests to Dr. Ortrud Vargas Hein MD, Department of Anesthesiology and Intensive Care, Medicine Charité—University Hospital Berlin, Charité Campus Mitte, Schumannstrasse 20/21, D-10117 Berlin, Germany. E-mail: ortrud.vargas@charite.de

elitis. The bypass grafts were all sufficient. A 23 mm mechanical Ultracor valve was placed in the aortic valve position and a 26 mm Carpentier ring was used for mitral valve reconstruction. The bypass time on CPB was 96 min and the aortic cross-clamp-time was 69 min. Due to known HIT II with a positive antibody-test, anticoagulation for CPB was performed using hirudin (Refludan, Aventis Pharma, Bad Soden am Taunus, Germany) following a fixed protocol (12). The patient obtained a bolus of 30 mg and a continuous hirudin infusion of 10–30 mg/h achieving a targeted hirudin concentration >4000 ng/mL. Fifty min before discontinuation of CPB hirudin was stopped and continuous HD with a polysulfone high-flux-filter (F80, surface area 1.8 m<sup>2</sup>, Fresenius Medical Care, Bad Homburg, Germany) and an initial dialysate rate of 15 L/h was initiated and continued postoperatively to filtrate hirudin. The hirudin concentration (Hirudin-Activity-Assay, DADE Behring, Marburg, Germany, cut-off 100 ng/mL) is presented in Fig. 1. During the operation the maximum of the aPTT was 186 s and the maximum of the international ratio (INR) of prothrombin time (PT) (STA, Roche Diagnostics, Mannheim, Germany) was 1.48. In the first 20 h after the operation the aPTT decreased from 107 to 78 s and the INR from 1.38 to 1.13. Because of excessive bleeding, transfusion of 27 packed red blood cells (PRBC), 39 fresh frozen plasma (FFP), and 8 platelet apheresis concentrates were required in the first 20 h after surgery. Seven hours after surgery re-thoracotomy was performed because of ongoing bleeding. No major bleeding site

was found. Minor bleeding sites were surgically treated. After re-thoracotomy and despite massive transfusion and continuous HD drainage loss continued in an average extent of 150 mL/h. Due to failure of conventional medical and surgical hemostasis, 60 µg/kg of rFVIIa were administered 20 h after surgery. Blood loss ceased completely within a few hours. Transfusion requirements were 4 PRBC and 2 platelet apheresis concentrates during the next 48 h. Hirudin anticoagulation was initiated 3 days after surgery when the aPTT decreased to 42 s. For anticoagulation of the mechanical valve and continuous HD, a bolus of 1–2 mg hirudin was applied every 2–3 days achieving a targeted aPTT of 40–50 s without further bleeding complications. The patient was transferred to a nonsurgical ICU of the same hospital for further weaning from the ventilator due to limited capacity in our ICU 10 days after surgery. Anticoagulation was accidentally initially performed with a total hirudin infusion of 43 mg/12 h. Under this dosage, hirudin concentration rose to 2269 ng/mL without causing any bleeding complications. The course of the patient was complicated by pneumonia (*Klebsiella pneumoniae*) requiring ventilator therapy. On day 24 the patient was transferred to a peripheral ward. He was neurologically without any new deficit. It was possible to mobilize him into a chair and he was able to eat and wash himself without any help. He was discharged on day 73.

## DISCUSSION

We report on a patient with chronic renal failure and HIT II who underwent combined cardiac re-do surgery using hirudin for CPB anticoagulation. The postoperative course in this patient was complicated by excessive and protracted hemorrhage. A stepwise approach of continuous HD, adequate substitution of blood products and rFVIIa was successful to manage bleeding.

In patients with a history of HIT II, renal failure, and in addition need of CPB and/or CRRT, anticoagulants like prostacyclin, danaparoid, bivalirudin, and argatroban have been used (13,14). In patients with a negative test on HIT II antibodies, an alternative choice for CPB is the use of high molecular weight (HMW) heparin in combination with a prostacyclin (13). This approach has been proved to be successful in a low number of case studies reported (13). However, high doses of prostacyclin necessary to achieve adequate inhibition of platelet activation cause severe vasodilation with the need for vaso-pressors (13). Regarding CRRT, prostacyclins seem to offer some advantages just in combination with

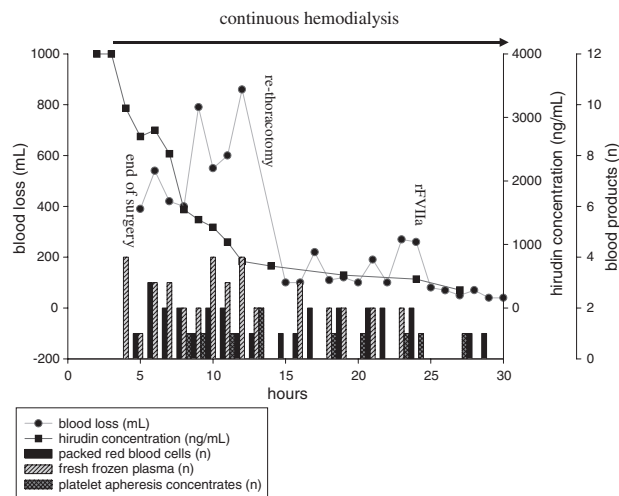


**FIG. 1.** Hirudin concentration, blood loss, and blood products in the intra- and postoperative period. rFVIIa—recombinant factor VIIa.

HMW heparin, excluding their use for patients with HIT II (14). Danaparoid applied for CPB and CRRT showed severe bleeding complications because of its long half-life which is even more prolonged in patients with renal failure (13,14). A promising alternative for anticoagulation during CPB and CRRT may be the direct thrombin inhibitor argatroban (14,15). This anticoagulant is eliminated through the liver with a half-life of 21–61 min and no cross-reactivity with HIT II antibodies (14). A few case-reports have shown preliminary satisfactory results regarding effectiveness and safety (9,14,15). Bivalirudin, another direct thrombin inhibitor, was successful for anticoagulation in cardiac surgery in a pilot study and single case reports and is currently under further evaluation in a phase 3 trial (9,13).

Alternative anticoagulation with hirudin for CPB in HIT II patients has been used successfully (2). However, in patients with renal insufficiency or failure bleeding complications after CPB occurred because of hirudin cumulation (2,3). In this case report, a high volume HD with a polysulfone high-flux-filter was instituted in the operating room after discontinuation of CPB in order to remove hirudin from plasma. In vitro studies demonstrated that high hirudin concentrations can be filtrated effectively whereas low hirudin concentrations persisted, as shown in this case report (5,6). Furthermore, other in vitro studies showed that the filtration of high hirudin concentrations is dependent on the high flux membrane used (16). A polysulfone membrane was superior to an AN69 membrane (16). However, observations in vivo have shown inconclusive results (16). Besides possible inadequate filtration of low hirudin concentrations, another reason for persisting low hirudin levels may have been the redistribution from the extravasal space (4,6). Hirudin is distributed 80% into the extravasal space (6). Correspondingly, aPTT values were persistently high. Another possible factor influencing persisting low hirudin levels could have been CPB. CPB induces alterations in the body fluid distribution (17) which could have had an additive effect on further hirudin extravasal distribution and following redistribution postoperatively. However, to our knowledge, no studies have been performed investigating hirudin distribution during and after CPB.

Re-do surgery per se is associated with a higher risk for bleeding complications (18,19). This fact together with the remaining low hirudin levels as well as the enormous blood losses led to a poor hemostatic capacity, possibly ending in disseminated intravascular coagulation. After re-thoracotomy blood losses were reduced but did not stop. On-going trans-

fusion requirements were necessary to achieve adequate cellular and plasmatic coagulation capacity.

In the situation of on-going bleeding rFVIIa was administered at a dose of 60 µg/kg to generate thrombin formation. Recombinant Factor VIIa at various dosages has been reported to be effective in refractory bleeding after cardiac surgery (10,11). Based on the hypothesis that the effect of a direct thrombin inhibitor might be counteracted by rFVIIa, it has recently been successfully used in a combined approach to treat bivalirudin-induced bleeding (9). In that approach, modified ultrafiltration was also not sufficient to stop bivalirudin-induced bleeding (9). After rFVIIa application blood loss and transfusion requirements were clearly reduced (9). Concerns about the use of rFVIIa for bleeding complications regarding possible thromboembolic complications remain and have been described in singular cases (20). Although safety and efficacy studies are far from complete, positive results in control of profuse bleeding predominate, as demonstrated in our patient (20).

After the third postoperative day anticoagulation for the mechanical valve could be achieved effectively with hirudin boli. Ten days after surgery the patient accidentally received high doses of hirudin without further bleeding complications. In contrast to the postoperative period, after wound healing or in nonsurgical patients, high hirudin concentrations seem not to have such deleterious bleeding consequences as immediately postoperatively. Postoperative bleeding complications after continuous application of hirudin for CRRT were described by Kern et al. whereas Fischer et al. administered hirudin continuously in nonsurgical patients for CRRT without bleeding complications (7,8).

In conclusion, successful treatment of a hirudin-induced bleeding after cardiac surgery may be achieved by using a stepwise approach of continuous HD, adequate substitution of FFP, platelets, and rFVIIa. Reoperation should be performed to elicit a possible surgical source of bleeding. Prospective studies are required to evaluate the efficacy and safety of this approach.

## REFERENCES

1. Claeys LG. Lethal heparin-associated pulmonary embolism—case reports. *Angiology* 2002;53:475–8.
2. Koster A, Hansen R, Kuppe H, Hetzer R, Crystal GJ, Mertzluft F. Recombinant hirudin as an alternative for anticoagulation during cardiopulmonary bypass in patients with heparin-induced thrombocytopenia type II. A 1-year experience in 57 patients. *J Cardiothorac Vasc Anesth* 2000;14:243–8.

3. Nuttall GA, Oliver WC Jr, Santrach PJ, et al. Patients with a history of type II heparin-induced thrombocytopenia with thrombosis requiring cardiac surgery with cardiopulmonary bypass: a prospective observational case series. *Anesth Analg* 2003;96:344–50.
4. Vanholder R, Camez A, Veys N, Van Loo A, Dhondt AM, Ringoir S. Pharmacokinetics of recombinant hirudin in hemodialyzed end-stage renal failure patients. *Thromb Haemost* 1997;77:650–5.
5. Bucha E, Kreml R, Nowak G. In vitro study of r-hirudin permeability through membranes of different haemodialysers. *Nephrol Dial Transplant* 1999;14:2922–6.
6. Willey ML, de Denus S, Spinler SA. Removal of lepirudin, a recombinant hirudin, by hemodialysis, hemofiltration, or plasmapheresis. *Pharmacotherapy* 2002;22:492–9.
7. Kern H, Ziemer S, Kox WJ. Bleeding after intermittent or continuous r-hirudin during CVVH. *Intensive Care Med* 1999;25:1311–4.
8. Fischer KG, Van de Loo A, Böhrler J. Recombinant hirudin (lepirudin) as anticoagulant in intensive care patients treated with continuous hemodialysis. *Kidney Int* 1999;56:46–50.
9. Stratmann G, de Silva AM, Tseng EE, et al. Reversal of direct thrombin inhibition after cardiopulmonary bypass in a patient with heparin-induced thrombocytopenia. *Anesth Analg* 2004; 98:1635–9.
10. Hendriks HGD, van der Maaten JMAA, de Wolf J, Waterbolk TW, Slooff MJ, van der Meer J. An effective treatment of severe intractable bleeding after valve repair by one single dose of activated recombinant factor VII. *Anesth Analg* 2001; 93:287–9.
11. von Heymann C, Hotz H, Konertz W, Kox WJ, Spies C. Successful treatment of refractory bleeding with recombinant factor VIIa after redo coronary artery bypass graft surgery. *J Cardiothorac Vasc Anesth* 2002;16:615–6.
12. Potzsch B, Hund S, Madlener K, Unkrig C, Muller-Berghaus G. Monitoring of recombinant hirudin: assessment of a plasma-based ecarin clotting time assay. *Thromb Res* 1997; 86:373–83.
13. Warkentin TE, Greinacher A. Heparin-induced thrombocytopenia and cardiac surgery. *Ann Thorac Surg* 2003;76:2121–31.
14. Vargas Hein O, Kox WJ, Spies C. Anticoagulation in continuous renal replacement therapy. *Contrib Nephrol* 2004;144: 308–16.
15. O'Shea SI, Ortel TL, Kovalik EC. Alternative methods of anticoagulation for dialysis-dependent patients with heparin-induced thrombocytopenia. *Semin Dial* 2003;16:61–7.
16. Frank RD, Farber H, Stefanidis I, Lanzmich R, Kierdorf HP. Hirudin elimination by hemofiltration: a comparative in vitro study of different membranes. *Kidney Int Suppl* 1999;72:S41–5.
17. Schumacher J, Eichler W, Heringlake M, Sievers HH, Klotz KF. Intercompartmental fluid volume shifts during cardiopulmonary bypass measured by A-mode ultrasonography. *Perfusion* 2004;19:277–81.
18. Delius RE, Walters HL 3rd. Re-operative surgery in pediatric patients. *Semin Thorac Cardiovasc Surg Pediatr Card Surg Annu* 2003;6:108–15.
19. McIlroy DR, Silvers AJ. Recombinant factor VIIa for life-threatening bleeding in high-risk cardiac surgery despite full-dose aprotinin. *Anesth Analg* 2004;99:27–30.
20. Ghorashian S, Hunt BJ. "Off-license" use of recombinant activated factor VII. *Blood Rev* 2004;18:245–59.

## Effect of the Electroporation in the Field Calculation in Biological Tissues

Airton Ramos

Electrical Engineering Department, Center of Technological Science, State University of Santa Catarina (UDESC), Joinville, Santa Catarina, Brazil

**Abstract:** This article presents results from the field calculation in a model of biological tissue taking into account the electroporation process. The electroporation model used in this study was proposed and experimentally verified by Glaser et al. for planar membranes. The numerical method for field calculation is based on a two-step process: (1) a cell-scale analysis, used for obtaining the field and current in a small volume containing only one cell and its nearest neighbors; and (2) a tissue-scale analysis, based on averaged values of conductivity and permittivity (obtained from the cell-scale analysis) and used for field calculation in a large volume of the tissue. The results for a high voltage applied between two electrodes in a two-dimensional analysis show that the electric field in the porated tissue extends beyond the limits obtained when the electroporation process is not taken into account. Furthermore, due to the electroporation, the tissue conductivity increases in the space between the electrodes. These results show that the electroporation process cannot be ignored in the field calculation in biological tissues when high strength electric fields are present. **Key Words:** Electroporation—Field calculation—Electrostimulation—Modeling and simulation.

Electroporation is a pore opening process that occurs in the plasmatic membrane of cells in a tissue when a high strength electric field is applied and the transmembrane voltage is increased to a value of the order of 1 Volt (1). The porated membrane can become temporarily permeable to the ionic and molecular components of the medium. Electroporation can be used for insertion of molecules such as DNA and proteins into cells and has been applied to increase the effectiveness of drugs such as bleomycin in tumor treatments by electrochemotherapy (2).

Although electroporation has been known and utilized for several years, it still lacks a formal theory to explain and quantify its physical mechanism. However, there is experimental evidence for pore formation and increases in conductance in lipidic membranes under high transmembrane voltage. Chang (3) used a rapid-freezing electron microscopy

---

Received August 2004; revised 2004.

Address correspondence and reprint requests to Dr. Airton Ramos, Universidade do Estado de Santa Catarina Centro de Ciências Tecnológicas, Departamento de Engenharia Elétrica, Campus Universitário Professor Avelino Marcante—Bairro Bom Retiro, Joinville, Santa Catarina, Brazil 89.223-100. E-mail: dee2ar@joinville.udesc.br

technique to obtain visual verification of the pore creation and evolution in human erythrocytes membranes excited by pulses of a DC shifted radio-frequency electric field. He observed that the pore distribution changed with time after applying the field. Glaser et al. (4) verified that planar lipidic membranes excited by electric field pulses increase their conductance with time, having a rate depending on the applied voltage. In the range of 0.65–1.5 V of the experiments, this dependence was observed to follow a well-defined rule, which can be expressed by the following equation:

$$\ln(\Delta I_m / \Delta t) = A + BV_m^2 \quad (1)$$

Where  $V_m$  and  $I_m$  are the transmembrane voltage and current, respectively, and  $\Delta t$  is the time length of the pulse. The values of the constants  $A$  and  $B$  were determined as  $-16$  and  $4.8 \text{ V}^{-2}$ , respectively, for membranes of asolectin (4).

Numerical simulation of the electric field distribution is a valuable tool in electrochemotherapy planning for estimating the extent of the electroporation. However, due to the absence of quantitative models of electroporation, previous work on numerical simulation of fields in biological tissues did not take into account this process (5). Electroporation increases the tissue conductivity close to the electrodes and the real field distribution is different from that calculated assuming that the tissue is homogeneous. In this paper we present some results obtained from numerical simulation of electroporation in a model of biological tissue using the Equivalent Circuit Method (ECM). In this work it is assumed that the Eq. 1 is valid for plasmatic membranes of cells at the beginning of the electroporation process. The main objective is to estimate the field and conductivity changes when electroporation is taken into account.

## MATERIALS AND METHODS

### The equivalent circuit method

The equivalent circuit method (ECM) (6) is based on modelling of the transport properties of the media by means of an electric circuit whose elements are associated with a discrete mesh of blocks that fill the analyzed space. The ECM has two approaches. The first is a cell-scale model, used for analysis of microscopic volumes containing a few cells, where the total current between two adjacent blocks in the mesh is described as having three components: conduction, diffusion, and shift current, which are modelled by circuit elements: conductance, current source, and capacitance, respectively. The second is a tissue-scale model, used for analysis of macroscopic volumes

containing large numbers of cells, where the equivalent circuit is based on the averaged values of the conductivity and permittivity inside the effective volume of a cell, so that, the circuit models the dispersive behavior of the tissue. In this approach, the equivalent circuit has conductances and capacitances that model the dominant first order relaxation process in a biological tissue (6).

The ECM consists in obtaining and analyzing the equivalent circuit of the media aiming to obtain the voltage and charge distributions in the space, in time steps, from specified initial and boundary conditions. The voltage is obtained from the computation of the node equations system and the charge is obtained by finite integration of the continuity equation in each block of the mesh.

### Numerical model for tissue electroporation

Since the electroporation process creates pathways across the lipidic matrix of the cell membranes, it can be considered as increasing both the conductivity and the diffusion coefficient for ions crossing the membranes. Since both processes in any media can be modeled by the ionic mobility, Glaser's experiments suggest that the ionic mobility in an electroporated membrane increases with the rate depending on the transmembrane voltage. We define the relative mobility ( $\lambda$ ) of any type of ion in the electrolyte surrounding the membranes by the quotient between the averaged mobility in the membrane and the mobility in water, that is,  $\lambda = \mu_m / \mu_w$ . Based on Eq. 1 we can write:

$$\frac{d\lambda}{dt} = \xi \exp\left(\frac{V_m^2}{V_p^2}\right) \quad (2)$$

where  $\xi$  and  $V_p$  are constants. This expression agrees with Glaser's model and experimental results, but it is only valid at the beginning of the electroporation processes.

The averaged effect of the process described by Eq. 2 is to increase the static conductivity of the tissue. Figure 1a shows the structure of a model tissue with cells of cubic shape. The static conductance is obtained as the equivalent of three contributions: conductance of the interstitial space ( $g_{so} = 2a\sigma_{so}$ ), conductance of the electrolyte ( $g_e = 2a\sigma_e$ ), and conductance of the membrane [ $g_m = (a^2/h)\sigma_m$ ]. Then, according to Fig. 1b, the equivalent static conductance is given by:

$$g_s = 2a \left[ \sigma_{so} + \frac{\lambda}{\lambda + \chi} \sigma_e \right] \quad (3)$$

where  $\sigma_{so}$  is the static conductivity of the intact tissue. The constant  $\chi$  would have a value of  $2h/a$  if the

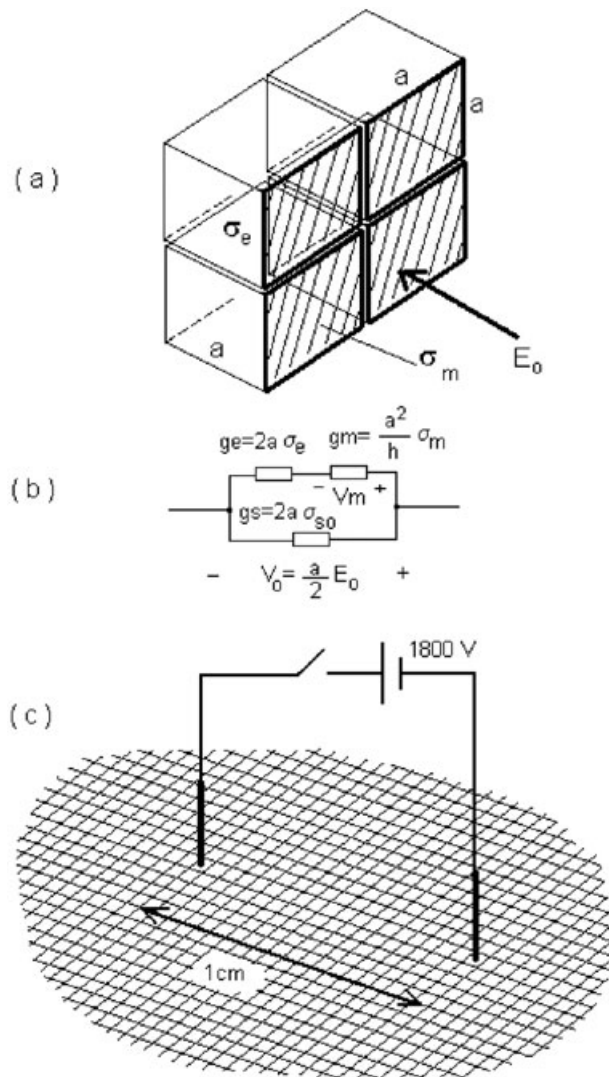


**FIG. 1.** (a) Details of a cubic cell tissue used in the cell-scale analysis. (b) Equivalent circuit for simulation of the electroporation in tissue-scale analysis. (c) Details of the two-dimensional structure used in the simulation of tissue electroporation.

electric field was uniformly distributed over the cell area. Since the field distribution can be obtained using the cell-scale model, it is possible to correct this value with numerical simulation. The transmembrane voltage can be calculated considering a voltage divider between  $g_e$  and  $g_m$ . Then,  $V_m$  can be given by:

$$V_m = \frac{(a/2)E_0}{1 + g_m/g_e} = \frac{\chi a/2}{\chi + \lambda} E_0 \quad (4)$$

where  $E_0$  is the applied electric field.

#### Numerical setup

The model tissue was built with cells of cubic shape. The electrolyte is an aqueous solution of two

ions,  $\text{Na}^+$  and  $\text{Cl}^-$ , with a concentration of 154 mM. The cell edge is 20  $\mu\text{m}$  with an interstitial width of 70 nm and membrane width of 10 nm. The cell scale analysis used a three-dimensional mesh of 14 000 blocks. The field source is a short pulse of voltage with duration of 30 ns applied between two electrodes in such a way that the electric field is 100 V/cm. It was performed 20 000 steps in the iterative method for cell-scale analysis with a time step of 0.3 ns, according to the rule for convergence given in (6). Based on the voltage and charge distributions around the cells, the averaged values of field and current were calculated and the conductivity and permittivity of the tissue were obtained. The parameters of Eq. 2 were estimated from Glaser's paper (constants A and B of Eq. 1). The values used in this work were  $\xi = 1 \times 10^{-11}$  and  $V_p = 0.46$  V. The tissue-scale analysis used a regular two-dimensional mesh with  $100 \times 100$  squares with 0.05 cm of edge. As shown in the Fig. 1c, electrodes were placed in the central region of the tissue and kept 1 cm apart. One pulse of 1800 V was applied during 50  $\mu\text{s}$  and the iterative process was performed in 167 000 steps of 0.3 ns. Based on the voltage and charge distributions, the field and current in the tissue were calculated.

## RESULTS

The dispersive parameters of the tissue obtained from cell-scale analysis are:  $\sigma_s = 5 \times 10^{-4}$  S/cm,  $\Delta\sigma = 1.9 \times 10^{-2}$  S/cm,  $\epsilon_\infty = 81$  e  $\Delta\epsilon = 1 \times 10^4$ . The obtained value for the constant  $\chi$  is  $1.33 \times 10^{-3}$ . Figure 2 shows the electric field distributions in the tissue at the end of the applied 1800 V pulse under electroporation occurrence and for the intact tissue. This figure also shows the distribution of conductivity.

## DISCUSSION

There are noticeable differences between the field distributions for the porated tissue and for the intact tissue. For the porated tissue the stimulated area is quite large and fields as high as 1000 V/cm or higher are not only concentrated around each electrode. Furthermore, in the electroporated tissue there are weak field areas at the back of each electrode, which are probably due to the high concentration of current and field in the high conductivity region between the electrodes. Also, in the porated tissue, the conductivity between the electrodes is higher than in the intact tissue and there is a correlation between the field and the conductivity distribution. According to Eq. 2, the conductivity increases faster in the places where the field is higher. We see that there is a maximum conductivity region of 19 mS/cm between the electrodes,

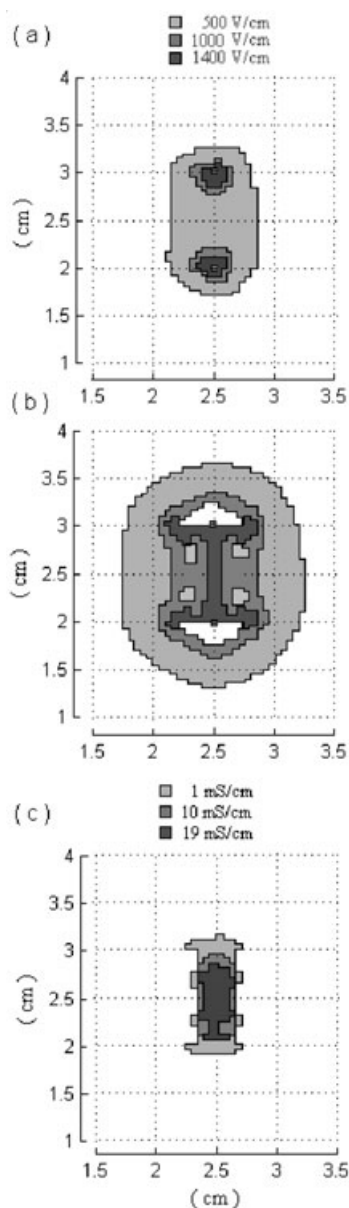


**FIG. 2.** Electric field distribution for a pulse of 1800 V during 50  $\mu$ s (a) without electroporation occurrence; (b) with electroporation occurrence; (c) conductivity distribution for the porated tissue. The positions of the electrodes are marked with "+" inside the little square. The legend shows the minimum values in the area indicated by the gray scale.

forming a high conductance channel. Since this value is equal to the electrolyte conductivity, it means that, due to the poration process, cell membranes have lost their ability to screen the ion displacement.

## CONCLUSION

The ECM method was used to study the field and conductivity distribution in a model of biological tissue excited by a short pulse of high voltage. Numerical results showed that the field distribution depends on the occurrence of electroporation of the plasmatic membranes and the increasing conductivity is higher in the space between the electrodes. Because of the electroporation processes, the tissue becomes inhomogeneous close to the electrodes. These results showed that the field calculation in biological tissue under high electrical fields should consider electroporation in order to take into account the conductivity changes of the media. This study was based on an electroporation model and experimental results for planar artificial membranes in the beginning of the electroporation process. Hence, numerical results should only be considered in a qualitative sense.

## REFERENCES

1. Tsong TY. On electroporation of cell membranes and some related phenomena. *Bioelectrochem Bioenergetics* 1990;24:291–5.
2. Hofmann GA. Electroporation therapy: a new approach for the treatment of head and neck cancer. *IEEE Transactions Biomed Engineering* 1999;46, 6:752–8.
3. Chang DC. Structure and dynamics of electric field-induced membrane pores as revealed by rapid-freezing electron microscopy. In: Chang D, Chassy BM, Saunders JA, Sowers, AE, eds. *Guide to Electroporation and Electrofusion*. San Diego, CA: Academic Press 1992:9–27.
4. Glaser RW, Leikin SL, Chernomordik LV, Pastushenko VF, Sokirko AI. Reversible electrical breakdown of lipid bilayers: formation and evolution of pores. *Biochim Biophys Acta* 1988;940:275–87.
5. Hofmann GA. Instrumentation and electrodes for in vivo electroporation. In: Jaroszeski MJ, Heller R, Gilbert R, eds. *Electrochemotherapy, Electroimmunotherapy, and Transdermal Drug Delivery*. Totowa, NJ: Humana Press 1999:37–61.
6. Ramos A, Raizer A, Marques JLB. A new computational approach for electrical analysis of biological tissues. *Bioelectrochem Bioenergetics* 2003;59:73–84.